The second point demonstrated by the present experiments is that the determination of transition-metal ordering is not difficult using only powder X-ray diffraction techniques. In the present calculation, the fixed atomic parameters and B factors of V_3S_4 were used, because the number of reflections sufficient to measure the accurate intensity was limited to seven, and was thus much less than the number of parameters to be determined. Even so, the reliability of the NOA model can obviously be recognized in the differences in R values (Table 1), and in the match of F_o and F_c, especially for reflections 002, 101, $\bar{2}02$ and 013, the structure factors of which are dominantly contributed to by the difference in the atomic scattering factors allocated to $M(1)$ and $M(2)$. This easy recognition of metal ordering suggests the possibility of investigating the behaviour of metal ordering 'at high temperatures'. This may elucidate the question of whether vacancy ordering and different metal ordering are coupled or are independent, because the *in situ* X-ray diffraction experiments at high temperature have so far concerned only vacancy ordering (*e.g.* Nakazawa, Saeki & Nakahira, 1975; Nakazawa, 1979; Wada, 1979*a*,*b*). The use of synchrotron-radiation X-rays may be particularly helpful in this context, because of tunability for a given wavelength and the intense flux.

The authors wish to thank Dr H. Nozaki, NIRIM, for his valuable discussions, Dr K. Yukino, NIRIM, and Dr I. Nakai, University of Tsukuba, for their support in setting up the diffractometer with a Cr target, and Professor M. Ohmasa, University of Tsukuba, for his critical reading of the manuscript.

References

ISHII, M., WADA, H., NOZAKI, H. & KAWADA, I. (1982). *Solid State Commun.* **42**, 605–608.
KAWADA, I., NAKANO-ONODA, M., ISHII, M., SAEKI, M. & NAKAHIRA, M. (1975). *J. Solid State Chem.* **15**, 246–252.
KAWADA, I. & WADA, H. (1981). *Phys. Status Solidi B*, **105**, 223–224.
NAKAZAWA, H. (1979). *Trans. Am. Crystallogr. Assoc.* **15**, 107–120.
NAKAZAWA, H., SAEKI, M. & NAKAHIRA, M. (1975). *J. Less-Common Met.* **40**, 57–63.
NOZAKI, H. & WADA, H. (1983). *J. Solid State Chem.* In the press.
NOZAKI, H., WADA, H. & YAMAMURA, H. (1982). *Solid State Commun.* **44**, 63–65.
TEMPLETON, D. H. (1962). *International Tables for X-ray Crystallography*, Vol. III, pp. 210–216. Birmingham: Kynoch Press.
WADA, H. (1978). *Bull. Chem. Soc. Jpn*, **51**, 1368–1373.
WADA, H. (1979*a*). *Bull. Chem. Soc. Jpn*, **52**, 2130–2135.
WADA, H. (1979*b*). *Bull. Chem. Soc. Jpn*, **52**, 2918–2922.
WADA, H. (1980). *Bull. Chem. Soc. Jpn*, **53**, 668–672.

Acta Cryst. (1983). B**39**, 535–542

Experimental Charge Density Study of Dicobalt Octacarbonyl* and Comparison with Theory

BY P. C. LEUNG AND P. COPPENS

Department of Chemistry, State University of New York at Buffalo, Buffalo, NY 14214, *USA*

(*Received* 23 *August* 1982; *accepted* 23 *February* 1983)

Abstract

The structure of dicobalt octacarbonyl, $Co_2(CO)_8$, has been redetermined at low temperature. Cell dimensions at 100 K are: a = 6·503 (1), b = 15·445 (2), c = 11·121 (1) Å and β = 90·57 (2)°. A significant difference between axial and equatorial Co–C bond lengths is observed which could not be seen at room temperature. The data have been refined with the aspherical-atom multipole formalism. Model maps based on the refinement results show the extension of the bridging C atom's lone-pair density in the plane containing the two Co atoms, in agreement with theoretical results predicting metal–metal bonding through the bridging ligand. d-Orbital populations derived from the refinement results agree well with theoretical values. The splitting of the 'e_g-type' levels is evident when the refinement is performed in a co-ordinate system fitted to the local pseudo octahedral symmetry.

Introduction

The structure determination of dicobalt octacarbonyl by Sumner, Klug & Alexander (1964) ended much speculation about the molecular geometry of this compound and showed that in the solid state two of the

* Di-μ-carbonyl-bis(tricarbonylcobalt).

0108-7681/83/050535-08$01.50

carbonyls are bridging, while each Co atom is also bonded to three terminal ligands. The unit cell contains two independent molecules, each of which is located on a crystallographic mirror plane of the $P2_1/m$ space group.

Several bonding schemes have been proposed for $Co_2(CO)_8$ and the related binuclear compound $Fe_2(CO)_9$. Sumner *et al.* (1964) proposed a simple pairing scheme which invokes a metal–metal bond directed along the line connecting the metal atoms to satisfy the 18-electron rule. The existence of a direct metal–metal bond in both compounds seems to have been quite generally accepted (Braterman, 1972; Cotton & Wilkinson, 1972, and other textbooks).

In $Co_2(CO)_8$ each metal atom contributes nine electrons, while the CO ligands add eight electrons to each of the Co's atomic orbitals. According to this line of reasoning the 18-electron rule is satisfied by combining either the two metal orbitals pointing along the metal–metal vector (d_{z^2}), leading to a straight bond, or two orbitals directed towards the empty bridging site, giving a bent bond, the other pair of atomic orbitals being doubly filled and constituting a lone pair on each of the atoms. In an analogous molecular-orbital scheme both bonding and antibonding states are filled for one of these two combinations, while the second, being singly filled, represents the metal–metal bonding.

Notwithstanding the elegance of this description and its success in explaining the molecule's diamagnetism, its validity has been undermined by recent calculations using the Hartree–Fock–Slater method, which have provided strong evidence that the bonding takes place exclusively through the bridging ligands. The crucial molecular orbitals spanning the metal–metal region are of a_1 and b_2 symmetry in the C_{2v} point group (coordinate system as indicated in Fig. 2, with the twofold axis of the molecule parallel to x). Though both a_1 orbitals are doubly occupied, the corresponding antibonding orbitals of b_2 symmetry are also populated, thus leading to an essentially zero net interaction.

The experimental study of the electron distribution in $Co_2(CO)_8$ presented here was undertaken to provide independent evidence on the nature of the bonding in this molecule. In addition to electron density maps comparison with theory is made at the level of the transition-metal atom's d-orbital populations which are obtained from the asphericity of the atomic charge distribution (Holladay, Leung & Coppens, 1983).

Experimental

Single crystals were grown by vacuum sublimation at 318 K, using material purchased from Ventron Chemical Corporation. Specimens obtained showed frequent twinning. Suitable single crystals were finally selected by careful scanning of reflection profiles. The crystal used in the room-temperature study was a parallelepiped of dimensions 0·22 × 0·32 × 0·44 mm along the a, b and c axes respectively. It was sealed in a Lindemann-glass capillary. The only systematic absence observed is $0k0$, $k = 2n$, in agreement with the space group $P2_1/m$ determined by Sumner *et al.* (1964). Data were collected on a FACS-I automatic Picker diffractometer with Zr-filtered Mo $K\alpha$ radiation. Intensity-collection information and unit-cell parameters are given in Table 1. Two crystals used in low-temperature data collection (100 K) were mounted on glass fibers and quickly introduced in the nitrogen stream to prevent decomposition. The first crystal with dimensions 0·75 × 0·33 × 0·39 mm was lost after collection of three symmetry-equivalent data sets up to $2\theta = 55°$, and two sets for the range $55 < 2\theta < 65°$. A second crystal with dimensions 0·40 × 0·18 × 0·25 mm was used to collect two symmetry-equivalent sets below $2\theta = 60°$ and one set with $60° < 2\theta < 95°$. In the second experiment the temperature was adjusted such that the unit-cell parameters matched those obtained for the first crystal. A small difference in unit-cell volume was nevertheless observed when a final refinement of the setting angles of 30 reflections was performed (Table 1).

Table 1. *Summary of crystallographic data and intensity-collection parameters*

	Room temperature, crystal 1	100 K, crystal 2	100 K, crystal 3
Space group	$P2_1/m$	$P2_1/m$	$P2_1/m$
a (Å)	6·632 (3)	6·482 (2)	6·503 (1)
b (Å)	15·630 (6)	15·398 (7)	15·445 (2)
c (Å)	11·336 (5)	11·087 (3)	11·121 (1)
β (°)	90·52 (3)	90·53 (2)	90·57 (2)
V (Å^3)	1174·9 (9)	1106·5 (6)	1116·9 (3)
Z	4	4	4
D_x (g cm^{-3})	1·934	2·053	2·034
D_m* (g cm^{-3})	1·87	—	—
μ_{calc} (cm^{-1})	29·63	31·47	31·42
Scan technique	θ–2θ	θ–2θ	θ–2θ
Scan width (°)	1·6 + 1·2 × cotg 2θ	1·8 + 0·9 × cotg 2θ	1·6 + 0·9 × cotg 2θ for $2\theta < 70°$; 2·0 + 1·1 × cotg 2θ for $2\theta > 70°$
Number of reflections measured	3673	12491	15399
Number of unique reflections	2807	4161	9776
R†	0·055	0·043	0·043
$(\sin\theta/\lambda)_{max}$ (Å^{-1})	0·65	0·76	1·04

* From Sumner *et al.* (1964).
† Internal consistency R factor, $R = \sum|F_o - \langle F\rangle|/\sum|F_o|$.

Conventional least-squares refinement

A least-squares refinement based on the structure as reported by Sumner *et al.* (1964) converged rapidly. Atomic scattering factors including those for

anomalous scattering of the Co, C and O atoms were taken as reported in *International Tables for X-ray Crystallography* (1974). In all refinements the quantity minimized was $\sum w^2[F_o^2 - (k^2F_c^2)]^2$ with $w = [\sigma^2_{\text{counting}} + (0{\cdot}02F_o^2)^2]^{-1}$. The two low-temperature data sets were absorption-corrected and then refined separately; they were subsequently merged using the least-squares scale factors. The data from the first set were corrected for isotropic extinction as determined by least squares ($y_{\min} = 0{\cdot}68$, $y = F_{\text{obs}}/F_{\text{corr}}$); extinction was negligible for the second set for which a smaller crystal was used. A joint refinement of the two data sets before merging included an isotropic difference temperature parameter. The value obtained (~0·0003 Å^2) was small, and equal to about 2% of the Co temperature parameters, indicating a reasonable temperature match notwithstanding the lack of exact agreement between the unit-cell results mentioned above. The more precise dimensions of the second crystal were used in the refinement of the joint data.

Table 2. *Summary of least-squares refinements*

	Room temperature	Low temperature			
		all-data, free-atom	high-order,* free-atom	multipole refinement with 4*s*, I	multipole refinement without 4*s*, II
$R(F^2)$ (%)	4·2	4·30	7·59	3·83	4·10
$R_w(F^2)$ (%)	5·8	7·43	8·72	6·54	6·61
S	1·66	1·39	1·23	1·23	1·24
NO	1797	5346	3426	5346	5346
NV	175	175	175	220	220

* $\sin\theta/\lambda > 0{\cdot}6$ Å^{-1}.

R factors for the refinement of the room-temperature data and all-data and high-order refinements of the merged low-temperature data are listed in Table 2.* The less accurate results of the room-temperature study will not be discussed further. Positional and thermal parameters are listed in Table 3, while interatomic distances and angles are given in Table 4. Atomic numbering is defined in Fig. 1.

Molecular dimensions

Each of the two independent molecules possesses approximate C_{2v} symmetry, with each Co atom being bonded to five carbonyl groups, one of which is an axial and the remainder are equatorial ligands (Fig. 1). According to the low-temperature results there is a statistically significant difference between the axial and equatorial Co—C(terminal) bond lengths which average 1·815 (1) and 1·832 (4) Å respectively (values from the high-order refinement, standard deviation from spread of individual values). It is noteworthy that a corresponding difference is not observed in the C—O bond lengths, which with average values of 1·138 (2) and 1·134 (4) Å are equal within experimental error. A similar difference between metal—carbonyl bond lengths is observed in dimanganese decacarbonyl [$Mn_2(CO)_{10}$] (Martin, Rees & Mitschler, 1982) in

* A list of structure factors has been deposited with the British Library Lending Division as Supplementary Publication No. SUP 38488 (48 pp.). Copies may be obtained through The Executive Secretary, International Union of Crystallography, 5 Abbey Square, Chester CH1 2HU, England.

Table 3. *Fractional positional parameters* (×10^4) *and anisotropic thermal parameters* (Å^2 × 10^4) (*high-order refinement*, $\sin\theta/\lambda > 0{\cdot}6$ Å^{-1})

	x	y	z	U_{11}	U_{22}	U_{33}	U_{12}	U_{13}	U_{23}
Co(1)	2437 (0·4)	1678 (0·1)	4480 (0·2)	144 (1)	107 (1)	148 (1)	3 (1)	−5 (1)	−7 (1)
Co(2)	−2476 (0·4)	1679 (0·1)	−834 (0·2)	165 (1)	118 (1)	141 (1)	1 (1)	13 (1)	14 (1)
TO(11)	1189 (5)	1010 (2)	2073 (2)	475 (13)	469 (11)	225 (7)	36 (9)	−114 (7)	−110 (7)
TO(21)	−3753 (6)	1125 (2)	1607 (2)	530 (15)	532 (13)	283 (8)	107 (12)	182 (9)	176 (9)
TO(12)	6489 (3)	786 (1)	4439 (2)	179 (6)	229 (6)	359 (8)	42 (5)	−4 (5)	−22 (5)
TO(22)	1512 (3)	735 (1)	−713 (2)	233 (7)	276 (7)	369 (8)	72 (6)	19 (6)	35 (5)
TO(13)	290 (3)	612 (1)	6290 (2)	326 (8)	202 (5)	274 (6)	−35 (5)	85 (5)	20 (4)
TO(23)	−4591 (4)	590 (1)	−2657 (2)	399 (10)	232 (6)	314 (7)	−65 (6)	−77 (7)	−60 (5)
BO(11)	4685 (5)	¼	6472 (2)	366 (12)	186 (7)	208 (7)	0	−133 (8)	0
BO(21)	−234 (5)	¼	−2807 (2)	376 (12)	175 (7)	227 (8)	0	146 (8)	0
BO(12)	−1590 (4)	¼	4131 (4)	152 (9)	204 (8)	618 (18)	0	−65 (9)	0
BO(22)	−6524 (4)	¼	−615 (3)	170 (9)	227 (8)	506 (14)	0	46 (8)	0
TC(11)	1680 (3)	1274 (1)	2993 (2)	257 (8)	251 (7)	171 (6)	31 (6)	−47 (5)	−45 (5)
TC(21)	−3247 (4)	1331 (1)	676 (2)	284 (9)	252 (7)	216 (7)	32 (6)	70 (6)	77 (5)
TC(12)	4974 (3)	1153 (1)	4427 (2)	166 (6)	151 (5)	216 (6)	6 (5)	1 (5)	−17 (4)
TC(22)	32 (3)	1128 (1)	−739 (2)	202 (7)	181 (5)	208 (6)	11 (5)	17 (5)	31 (4)
TC(13)	1106 (3)	1029 (1)	5597 (2)	193 (6)	136 (5)	206 (6)	−9 (5)	23 (5)	−8 (4)
TC(23)	−3792 (3)	1016 (1)	−1954 (2)	245 (7)	155 (5)	209 (6)	−7 (5)	−8 (5)	−11 (4)
BC(11)	3659 (4)	¼	5602 (2)	198 (9)	124 (6)	161 (7)	0	−33 (6)	0
BC(21)	−1245 (4)	¼	−1942 (2)	236 (10)	136 (6)	148 (7)	0	49 (7)	0
BC(12)	193 (4)	¼	4315 (2)	149 (9)	144 (7)	287 (10)	0	−13 (7)	0
BC(22)	−4750 (4)	¼	−744 (2)	166 (9)	153 (7)	243 (9)	0	9 (7)	0

Table 4. *Molecular geometry of* $Co_2(CO)_8$

(*a*) Distances (Å)

	All data	High order		All data	High order		All data	High order
Co(1)–Co(1′)	2·5301 (8)	2·5293 (8)	Co(1)–BC(11)	1·940 (1)	1·938 (2)	TC(13)–TO(13)	1·134 (1)	1·136 (3)
Co(2)–Co(2′)	2·5278 (8)	2·5276 (8)	–BC(12)	1·937 (1)	1·935 (2)	TC(23)–TO(23)	1·135 (1)	1·139 (2)
			Co(2)–BC(21)	1·939 (1)	1·939 (2)			
Co(1)–TC(11)	1·826 (1)	1·826 (2)	–BC (22)	1·942 (1)	1·945 (2)	BC(11)–BO(11)	1·165 (2)	1·167 (3)
–TC(12)	1·835 (1)	1·834 (2)				BC(12)–BO(12)	1·167 (2)	1·172 (3)
Co(2)–TC(21)	1·832 (1)	1·833 (2)	TC(11)–TO(11)	1·137 (1)	1·140 (2)	BC(21)–BO(21)	1·164 (2)	1·167 (3)
–TC(22)	1·839 (1)	1·836 (2)	TC(12)–TO(12)	1·135 (1)	1·132 (3)	BC(22)–BO(22)	1·162 (2)	1·160 (4)
			TC(21)–TO(21)	1·132 (1)	1·132 (3)			
Co(1)–TC(13)	1·817 (1)	1·816 (2)	TC(22)–TO(22)	1·136 (1)	1·134 (3)			
Co(2)–TC(23)	1·816 (1)	1·815 (2)						

(*b*) Angles (°)

Co(1)–BC(11)–Co(1′)	81·41 (6)	BC(11)–Co(1)–TC(13)	96·53 (5)	Co(1)–TC(13)–TO(13)	178·69 (8)
Co(1)–BC(12)–Co(1′)	81·54 (7)	BC(12)–Co(1)–TC(13)	93·62 (5)	Co(2)–TC(23)–TO(23)	178·92 (9)
Co(2)–BC(21)–Co(2′)	81·34 (6)	BC(21)–Co(2)–TC(23)	97·30 (5)		
Co(2)–BC(22)–Co(2′)	81·22 (7)	BC(22)–Co(2)–TC(23)	93·00 (5)	Co(1)–BC(11)–BO(11)	139·25 (3)
				Co(1)–BC(12)–BO(12)	139·15 (3)
BC(11)–Co(1)–TC(11)	154·98 (5)	TC(11)–Co(1)–TC(12)	93·16 (5)	Co(2)–BC(21)–BO(21)	139·32 (3)
BC(12)–Co(1)–TC(12)	163·52 (5)	TC(21)–Co(1)–TC(22)	93·47 (5)	Co(2)–BC(22)–BO(22)	139·31 (3)
BC(21)–Co(2)–TC(21)	152·44 (5)	TC(11)–Co(1)–TC(13)	107·87 (5)	BC(11)–Co(1)–BC(21)	86·49 (6)
BC(22)–Co(2)–TC(22)	165·35 (5)	TC(12)–Co(1)–TC(13)	102·13 (5)	BC(21)–Co(2)–BC(22)	85·77 (6)
		TC(21)–Co(2)–TC(23)	109·35 (5)		
BC(11)–Co(1)–TC(12)	86·91 (5)	TC(22)–Co(2)–TC(23)	100·98 (5)	TC(13)–Co(1)–Co(1′)	123·33 (3)
BC(12)–Co(1)–TC(11)	86·52 (5)			TC(23)–Co(2)–Co(2′)	124·25 (3)
		Co(1)–TC(11)–TO(11)	178·81 (11)		
BC(21)–Co(2)–TC(22)	88·12 (5)	Co(1)–TC(12)–TO(12)	175·63 (9)		
BC(22)–Co(2)–TC(21)	85·92 (5)	Co(2)–TC(21)–TO(21)	178·24 (11)		
		Co(2)–TC(22)–TO(22)	174·86 (9)		

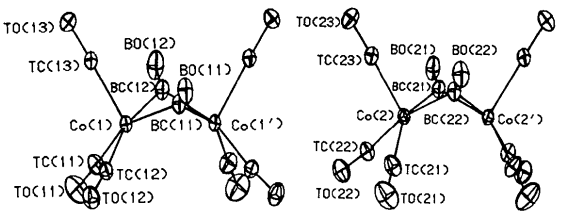

Fig. 1. Labelling of atoms and thermal ellipsoids of the two independent molecules in the unit cell.

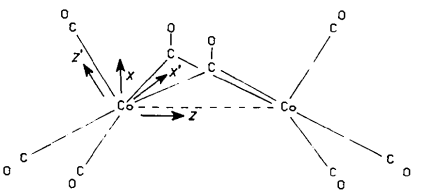

Fig. 2. Definition of Co local coordinate systems used in the multipole refinements. For all carbonyl groups the *z* axis is along the C–O bond pointing from O to C. The *x* axis for the bridging carbonyl is in the plane of Co atoms.

which the uncorrected Mn–CO bond lengths are 1·815 (2) and 1·856 (1) Å in the axial and equatorial directions respectively. This larger difference is translated, in this case, into a change in C–O distance from 1·146 (3) to 1·138 (3) Å. As the CO bond-length variation is smaller by a factor of about five, the absence of a significant difference in $Co_2(CO)_8$ is as predicted.

Charge density refinement

After completion of the conventional refinement the structure was refined further using the atomic multipole formalism as described by Hansen & Coppens (1978). The local coordinate system on each atom is defined in Fig. 2. In most refinements a Co reference frame related to the C_{3v} symmetry of $Fe_2(CO)_9$ was used; in addition, refinements were performed in a coordinate system adapted to the (approximate) local C_{4v} symmetry with the axial ligand oriented along the fourfold axis. In all refinements *m* symmetry is imposed on the Co atoms, while all terminal carbonyls are constrained to be equivalent and to have C_∞ symmetry.

Because of the difficulty of refining the 4*s* electrons (see, for example, Stevens, DeLucia & Coppens, 1980), two different valence states were tested corresponding to the (18-electron core)$(3d)^x$ and (18-electron core)-$(3d)^x(4s)^2$ configurations, x being a least-squares variable. In these refinements the spherical valence shell components have the radial dependence of the corresponding HF shells modified by a κ parameter (Coppens, Guru Row, Leung, Stevens, Becker & Yang, 1979), while the multipole deformation functions have a Slater-type radial dependence of the form $r^n \exp(-\zeta r)$; with $n = 4$ for Co and $n = 2, 3, 4, 4$ for $l = 1, 2, 3$ and 4

respectively, for C and O atoms. Higher R factors were obtained in test refinements with a Slater-type radial dependence for all valence electrons. As shown in Table 2, R factors are slightly lower for refinements I in which 4s electrons are included. Metal-atom population parameters are reported in Table 5. d-Orbital occupancies derived from the population parameters (Holladay, Leung & Coppens, 1983) are given in Table 6.

Two sets of density maps were calculated after each refinement. Residual maps, based on $(F_{obs}/k - F_{calc})$, represent electron density features that have not been described by the modeling functions. Though the residual maps are noisy (see, for example, Fig. 3a), features disappear by averaging over chemically equivalent sections except for a diffuse ring of charge around the Co atoms and charge accumulation at the bond midpoint (Fig. 3b), which appear in all equivalent sections.

The model maps, based on $(F_{\text{calc, multipole model 1}} - F_{\text{spherical atom}})$ represent the dynamic deformation density as described by the model-fitting functions. They are shown in three different planes. In plane I (Fig. 4) containing two Co atoms and the axial carbonyls the metal-atom density is polarized in a direction away from the carbonyl ligand towards the empty bridging site. The lone-pair density of the C atom and the C—O density are clearly visible. However, neither here nor in the other planes containing carbonyl ligands is the O lone-pair density observed. A similar observation is made for $Co_3(CO)_9CH$ (Leung & Coppens, to be published), for which a fragment difference map, in which the thermally smeared theoretical density of the CO fragment is subtracted from the experimental density, shows a strong depletion of density in the O lone-pair region of the bonded CO molecule. In plane II (Fig. 4), containing the Co atoms and the bridging carbonyl, the polarization of the metal density is again evident. The density at the back of the bridging carbonyl C atom is clearly elongated parallel to the Co—Co vector. This elongation, which is not observed in the perpendicular plane through the bridging carbonyl (plane III, Fig. 4), is indicative of the metal—ligand interaction distorting the cylindrical symmetry of the free CO molecule as discussed further below.

The average standard deviation of the total density which is representative of the error in the deformation density at positions away from the atoms (Stevens & Coppens, 1976) is calculated to be 0·11 e Å^{-3} before averaging over equivalent sections. The fact that most features in the residual maps are below 3σ indicates

Table 5. *Population parameters, refinement with 4s electrons*

TO = terminal oxygen, BO = bridging oxygen, TC = terminal carbonyl, BC = bridging carbonyl.

	Co	TO	BO	TC	BC
κ	0·996 (9)	1·002 (3)	1·002 (4)	1·015 (3)	1·009 (5)
ζ	7·88 (22)	3·20 (8)	1·82 (16)	3·18 (6)	2·92 (12)
y_{00}	7·10 (3)	6·14 (2)	5·98 (3)	3·87 (3)	3·90 (3)
y_{11}	−0·15 (2)				
y_{10}	0·05 (2)	0·21 (2)	0·15 (5)	0·17 (2)	0·02 (2)
y_{20}	0·09 (1)	0·17 (1)	0·17 (4)	0·37 (2)	0·36 (2)
y_{21}	−0·02 (1)				
y_{22}	0·07 (1)		−0·03 (3)		0·11 (2)
y_{30}	0·03 (1)	0·06 (2)	0·02 (6)	−0·06 (2)	−0·18 (2)
y_{31}	0·06 (1)				
y_{32}	0·01 (1)		−0·01 (4)		0·10 (2)
y_{33}	0·00 (1)				
y_{40}	0·04 (3)				
y_{41}	0·02 (1)				
y_{42}	0·03 (2)				
y_{43}	0·12 (2)				
y_{44}	0·02 (2)				

Table 6. *Orbital populations*

See Fig. 2 for definition of coordinate systems.

	Experimental				Theoretical*		Experimental† C_{4v} coordinate system	
	with 4s		without 4s					
d_{z^2}	1·57 (4)	22·0%	1·67 (4)	21·7%	1·53	21·2%	1·38 (3)	19·5%
$d_{x^2-y^2}$	1·53 (4)	21·5	1·61 (3)	20·9	1·49	20·7	1·48 (3)	20·9
d_{xy}	1·34 (4)	18·8	1·46 (3)	19·0	1·31	18·4	1·20 (3)	16·9
d_{xz}	1·36 (3)	19·1	1·50 (3)	19·5	1·55	21·5	1·53 (3)	21·6
d_{yz}	1·31 (3)	18·4	1·46 (3)	19·0	1·33	18·4	1·50 (3)	21·2
Total d	7·11 (3)		7·70 (3)		7·21		7·09 (3)	
4s	2		0		−0·02		2	
$4p_x$					0·16			
$4p_y$					0·04			
$4p_z$					0·35			

* Gross orbital populations as given by Heijser (1979).

† See Fig. 2 for the alternative coordinate system. Note that the values in this column *cannot* be compared directly with the other entries in the table because of the different definition of axes.

Fig. 3. Averaged residual maps and typical residual maps before averaging in the order I, II, III, IV. Plane I: containing two Co atoms and the axial carbonyls. Plane II: containing the Co atoms and the bridging carbonyls. Plane III: containing the bridging carbonyls. Plane IV: through two terminal carbonyl groups. (*a*) Individual residual maps. (*b*) Averaged residual maps. Contours 0·1 e Å^{-3}, zero and negative contours broken.

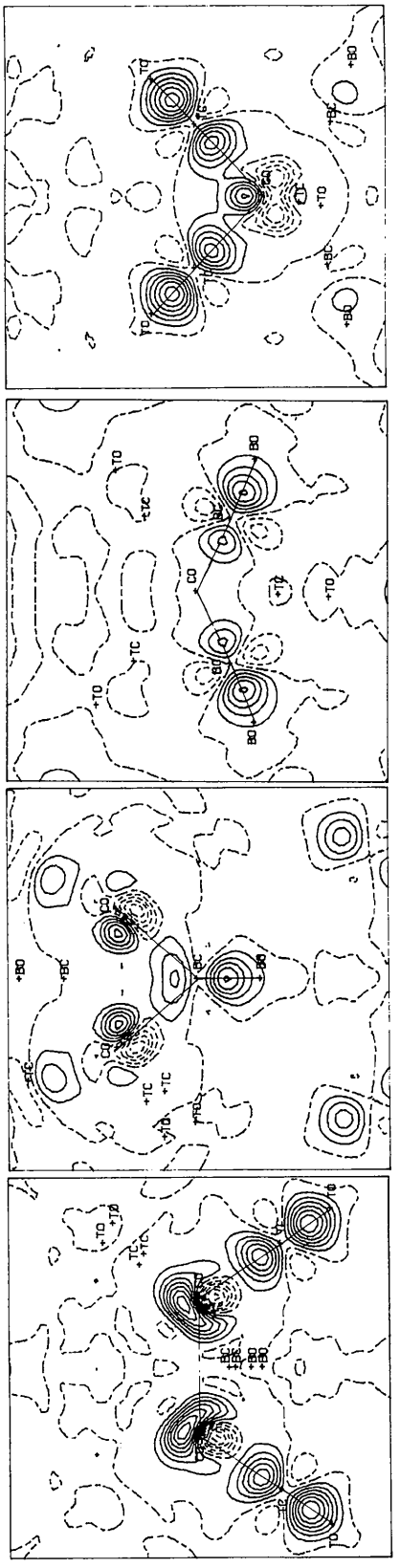

Fig. 4. Model maps in the planes as defined in Fig. 3. Contours 0·1 e Å^{-3}.

that the fit obtained in modeling the deformation density is adequate. The main exception is the peak at the Co–Co midpoint in the mirror plane. The standard deviation at this special position is 0·15 e Å^{-3} which is considerably lower than the peak height of about 0·7 e Å^{-3} observed at both crystallographically independent positions.

Discussion of bonding in $Co_2(CO)_8$

According to the molecular-orbital calculations with the LCAO–HFS (Hartree–Fock–Slater) method by Heijser (1979) and Heijser, Baerends & Ros (1980) the stability of the metal dimer is due to the interaction of metal e'_g orbitals (of approximate C_{3v} symmetry) with the $2\pi_{\parallel}$ orbital of the bridging carbonyl, leading to three-center Co($3d,e'_g$)–C$2\pi_{\parallel}$–Co($3d,e'_g$) bonds through the bridging ligands. The orbital maps for the occupied $13a_2$ and $24b_2$ MO's as reported by Heijser *et al.* support this interpretation as they show continuous, nodeless, regions between the Co atoms and the bridging C atoms. Direct metal–metal bonding as suggested by the qualitative description discussed earlier does not occur, however. As the metal orbitals pointing along the pseudo threefold axis are low-lying ('t_{2g}-type') orbitals, they combine into low-lying molecular orbitals. As a result both bonding (a_1) and antibonding (b_2) combinations are occupied. The same is true for the combination of the e'_g-type Co orbitals pointing toward the empty bridging site. The $29a_1$ orbital which represents the bent bond is occupied, but this is also true for its antibonding counterpart the $24b_2$ orbital, which is the highest occupied molecular orbital (Fig. 5). The conclusion is reached that the stability of the complex is due to two-electron three-center bonding.

Such a through-ligand interaction between the metal atoms is supported by the observed extension of the C 'lone-pair' peak in the plane of the Co atoms. Comparison of experimental and theoretical *d*-orbital occupancies (Table 6) provides additional quantitative support for the calculations. The only appreciable discrepancy is observed for d_{xz} orbitals which are depopulated relative to the spherical atom according to the experiment and contain more than 20% of the *d* electrons according to the theory. Since this is the orbital which makes a large contribution to the $24b_2$ three-center metal–metal bonding MO (it has 46·1% d_{xz} character according to the calculation), the d_{xz} orbital character of this bonding combination may have been overestimated by the calculation.

The multipole refinement with 4*s* electrons was also performed in an alternative coordinate system (Fig. 1, primed axes) in which the *z* axis is along the axial CO ligand. As expected, *R* factors obtained are identical to those of refinement I. This coordinate system is more suited for an analysis of the Co atom's asymmetry; the

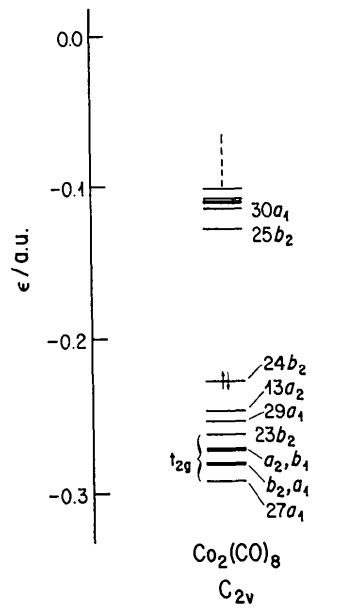

Fig. 5. Orbital energies according to Heijser *et al.* The six lowest orbitals are combinations of t_{2g}-type orbitals on the metal atoms. The highest occupied molecular orbital (HOMO) is indicated by the ↑↓ symbol.

d_{xy} and d_{z^2} orbitals correlate with the e_g orbitals in octahedral site symmetry. The results (Table 6) show the d_{xy} orbital, which points towards the equatorial ligands, to be most depopulated, and thus more destabilized, than the d_{z^2} orbital which is only directed towards the axial ligand and towards the void of the empty bridging site. This indication of level splitting is in clear agreement with crystal-field theory. Both orbitals are depopulated relative to the t_{2g}-type orbitals.

The lack of density in the model maps near the Co—Co midpoint results from the absence of functions spanning this region in the multipole model. Though the theoretical deformation maps published by Heijser (1979) do not show density in this region, the X-ray residual maps indicate peaks of about 0·7 e Å^{-3}. It seems unlikely that these peaks are a result of covalent bonding. They are much sharper than what would be expected on the basis of *d*-orbital overlap. Even in $Mn_2(CO)_{10}$ in which a direct metal–metal bond exists, density accumulation at the bond midpoint can only be observed when prepared $Mn(CO)_5$ fragments are subtracted. Even then the peak in the theoretical fragment deformation map is only about 0·10 e Å^{-3}. It is possible that the peaks at Co—Co bond midpoints are due to an accumulation of experimental errors. Explanations advanced for extra peaks near transition-metal atoms include thermal stress (Troup, Extine & Ziolo, 1982) and inadequate absorption correction (Coppens, 1982). Such peaks are often disposed symmetrically around the transition-metal atom. In the case of $Co_2(CO)_{10}$ features observed in the back of both Co atoms with a height of about 0·3 e Å^{-3} at about half the Co—Co bond distance (Fig. 3) may combine between the Co atoms to lead to a peak of double height as is indeed observed.

Conclusions

The experimental study reported here generally supports theoretical results which indicate strong through-ligand metal–metal interactions. The almost quantitative agreement between experimental and theoretical *d*-orbitals' occupancies is satisfying given the completely different nature of the two methods.

Support of this work by the National Science Foundation (CHE 7905897) is gratefully acknowledged.

References

BRATERMAN, P. S. (1972). *Struct. Bonding (Berlin)*, **10**, 57–87.
COPPENS, P. (1982). *ACA Program Abstr. Ser.* 2, **10**, 25.
COPPENS, P., GURU ROW, T. N., LEUNG, P., STEVENS, E. D., BECKER, P. J. & YANG, Y. W. (1979). *Acta Cryst.* A**35**, 63–72.
COTTON, F. A. & WILKINSON, G. (1972). *Advanced Inorganic Chemistry*, 3rd ed. New York: Interscience.
HANSEN, N. K. & COPPENS, P. (1978). *Acta Cryst.* A**34**, 909–921.
HEIJSER, W. (1979). Thesis, Free Univ. Amsterdam, The Netherlands.
HEIJSER, W., BAERENDS, E. J. & ROS, P. (1980). *Faraday Discuss. Chem. Soc.* **14**, 211–234.
HOLLADAY, A., LEUNG, P. & COPPENS, P. (1983). *Acta Cryst.* A**39**, 377–387.
International Tables for X-ray Crystallography (1974). Vol. IV. Birmingham: Kynoch Press.
MARTIN, M., REES, B. & MITSCHLER, A. (1982). *Acta Cryst.* B**38**, 6–15.
STEVENS, E. D. & COPPENS, P. (1976). *Acta Cryst.* A**32**, 915–917.
STEVENS, E. D., DELUCIA, M. L. & COPPENS, P. (1980). *Inorg. Chem.* **19**, 813–820.
SUMNER, G. G., KLUG, H. P. & ALEXANDER, L. E. (1964). *Acta Cryst.* **17**, 732–742.
TROUP, J. M., EXTINE, M. W. & ZIOLO, R. F. (1982). *Electron Distributions and The Chemical Bond*, edited by P. COPPENS & M. B. HALL, pp. 285–296. London, New York: Plenum.